Hot-carrier degradation caused interface state profile—Simulation versus experiment

I. Starkov[a)]
Christian Doppler Laboratory for Reliability Issues in Microelectronics at the Institute for Microelectronics, TU Wien, Gußhausstraße 27-29, A-1040 Wien, Austria

S. Tyaginov
Institute for Microelectronics, Technische Universität Wien, Gußhausstraße 27-29, A-1040 Wien, Austria

H. Enichlmair
Department of Process Development and Implementation, Austriamicrosystems AG, Unterpremstaetten, Tobelbader Straße 30, A-8141, Austria

J. Cervenka
Institute for Microelectronics, Technische Universität Wien, Gußhausstraße 27-29, A-1040 Wien, Austria

C. Jungemann
Institute for Microelectronics and Circuit Theory, Bundeswehr University, Werner-Heisenberg-Weg 39, 85577 Munich, Germany

S. Carniello and J. M. Park
Department of Process Development and Implementation, Austriamicrosystems AG, Unterpremstaetten, Tobelbader Straße 30, A-8141, Austria

H. Ceric
Christian Doppler Laboratory for Reliability Issues in Microelectronics at the Institute for Microelectronics, TU Wien, Gußhausstraße 27-29, A-1040 Wien, Austria

T. Grasser
Institute for Microelectronics, Technische Universität Wien, Gußhausstraße 27-29, A-1040 Wien, Austria

(Received 10 August 2010; accepted 15 December 2010; published 19 January 2011)

Hot-carrier degradation is associated with the buildup of defects at or near the silicon/silicon dioxide interfaced of a metal-oxide-semiconductor transistor. However, the exact location of the defects, as well as their temporal buildup during stress, is rarely studied. In this work we directly compare the experimental interface state density profiles generated during hot-carrier stress with simulation results obtained by a hot-carrier degradation model. The developed model tries to capture the physical picture behind hot-carrier degradation in as much detail as feasible. The simulation framework includes a transport module, a module describing the microscopic mechanisms of defect generation, and a module responsible for the simulation of degraded devices. Due to the model complexity it is very important to perform a thorough check of the output data of each module before it is used as the input for the next module. In this context a comparison of the experimental interface state concentration observed by the charge-pumping technique with the simulated one is of great importance. Obtained results not only show a good agreement between experiment and theory but also allow us to draw some important conclusions. First, we demonstrate that the multiple-particle mechanism of Si–H bond breakage plays a significant role even in the case of a high-voltage device. Second, the absence of the lateral shift of the charge-pumping signal means that no bulk oxide charge buildup occurs. Finally, the peak of interface state density corresponds to the peak of the carrier acceleration integral and is markedly shifted from typical markers such as the maximum of the electric field or the carrier temperature. This is because the degradation is controlled by the carrier distribution function and simplified schemes of hot-carrier treatment (based on the mentioned quantities) fail to describe the matter. © *2011 American Vacuum Society.* [DOI: 10.1116/1.3534021]

I. INTRODUCTION

Transistors of practically all technology nodes suffer from hot-carrier degradation (HCD) (see Refs. 1–5). This detrimental phenomenon has been known for more than four decades and numerous modeling attempts have been undertaken (see Refs. 1–3 and references therein). Although a considerable number of HCD models have been proposed, most of them are empirical/phenomenological and only a limited number of physics-based models exist. One may distinguish two main approaches focused on this matter: the

a)Electronic mail: starkov@iue.tuwien.ac.at

Author complimentary copy. Redistribution subject to AIP license or copyright, see http://jvb.aip.org/jvb/copyright.jsp

reaction-diffusion-based model[6,7] and the Hess model[8,9] which has been recently extended by Bravaix and co-workers.[4,5]

Both models relate the degradation to the buildup of interface states by breaking passivated Si–H bonds. The first model is an adaptation of the reaction-diffusion framework—which is the most popularized explanation for the negative bias temperature instability (NBTI) (Refs. 10–12)—to the case of HCD. According to this approach, the difference in time exponents describing NBTI and HCD originates from the one-dimensional diffusion typical for the former case versus the two-dimensional one occurring in the latter situation. However, as has been repeatedly noted (see, e.g., Refs. 13 and 14) this concept fails to properly account for the recovery of NBTI induced degradation. As such, its extension and application to HCD appear doubtful. This is mostly because a reaction-diffusion-based HCD model would allow for complete recovery of the degradation within reasonable time scales, something not observed experimentally.

We, therefore, follow the Hess strategy, which has already been demonstrated to capture many hot-carrier degradation peculiarities. Among them are the isotope effect revealed in hydrogen-versus deuterium-annealed devices,[15] explanation of the change of the HCD worst-case conditions observed in scaled devices,[16] as well as the double-power law of the degradation time dependence,[17] which can be explained by introducing two types of the mechanisms triggering the Si–H bond breakage. These mechanisms are the single-particle (SP) and multiple-particle (MP) processes. The SP mechanism assumes that the bond is broken by a solitary particle with sufficiently high energy. This scenario is dominant in long channel and/or high-voltage devices with rather high operating voltages. Since the essential requirement of transistor scaling is the supply voltage reduction, starting from a certain node carriers in the transistors become "cold" in terms of triggering the SP process. Therefore, a series of interactions between the bond and colder carriers is required to excite the bond into a sufficiently distorted state to allow for hydrogen release and bond dissociation. This MP mechanism dominates the degradation at low supply voltages.[4,5,8,9]

The main shortcoming of models based on this concept is that they have been applied in a macroscopic manner and do not properly account for the microscopic details responsible for the interface state buildup. An attempt in bridging the gap between the microscopic and the device level has been undertaken.[18] However, this approach does not consider the details of the interface trap generation mechanism and thus appears somewhat phenomenological.

As has been reported previously,[9] the Si–H bond breakage is controlled by the interplay of the SP and MP mechanisms which are associated with the "hot" and "colder" carriers. Therefore, for proper modeling of HCD, detailed information about the carrier energy distribution function (DF) is required, as the DF determines the reaction rates and sensitively depends on the applied bias conditions, temperature, and device topology. Using this information one can then proceed to properly describe defect buildup which eventually results in a change of the device characteristics. In other words, a comprehensive hot-carrier degradation model should include three essential modules: (i) a treatment of carrier transport for the particular device architecture, bias conditions, and temperature; (ii) consideration of the physical mechanisms responsible for defect generation; and (iii) simulation of the electrical characteristics of the degraded devices.

The model of Hess provides a clear link to the microscopic defect creation process.[8,9] However, it requires detailed knowledge of the carrier distribution function. So far, the carrier distribution function has not been rigorously evaluated. Instead, it has been replaced by phenomenological relations using technology computer-aided design (TCAD) simulations in Ref. 18. Alternatively, Bravaix and co-workers[4,5] proposed a hybrid model considering the microscopic mechanisms but treating them phenomenologically by substituting the precise assessment of the DF by some empirical factors. Such an approach—of course—cannot reflect the real microscopic picture of the matter. For instance, the question about the lateral defect position along the interface cannot be properly addressed within this framework.

In our recent works[19,20] we used an extended version of the Hess model. Particular emphasis has been placed on an accurate evaluation of the distribution function using the full-band Monte Carlo device simulator MONJU.[21] Based on that input, the interface trap density N_{it} is calculated using a superposition of the SP and MP mechanisms. These N_{it} profiles (calculated for each time step) are used as input data for our device simulator MINIMOS-NT (Ref. 22) which is employed to model the characteristics of the degraded device. Although good agreement between experiment and calibrated theory has been achieved, the results of the model should be carefully checked for their consistency.

As stated before, a physics-based model for hot-carrier degradation includes three main modules. Each module is based on some assumptions acting as potential sources of error and includes a certain number of fitting parameters. Due to the complicated structure of the model these errors should be screened by properly evaluating the interfaces between the modules. Therefore, although a good representation of the degraded device characteristics could be achieved, we attempt to verify the microscopic model for the defect buildup in the following by employing charge-pumping (CP) data for a particular device architecture. It is worth emphasizing that the algorithms for extraction of the N_{it} profiles versus position from the CP data are based on some assumptions and thus could be potentially inaccurate as well. Therefore, we carry out a thorough comparison between simulated N_{it} profiles and those extracted from CP data. Such a comparison followed an elimination of potential errors related to each simulation module is the main goal of this paper.

The text is organized as follows: after the introduction, the microscopic model for hot-carrier induced interface state creation is presented (Sec. II), followed by the sample and

Author complimentary copy. Redistribution subject to AIP license or copyright, see http://jvb.aip.org/jvb/copyright.jsp

experimental setup as well as the techniques for CP data processing descriptions (Sec. III). The obtained N_{it} profiles are compared and discussed in Sec. IV.

II. MICROSCOPIC MODEL FOR INTERFACE STATE CREATION

Under hot-carrier stress conditions both SP and MP mechanisms are present and their interplay is described by the shape of the distribution function, which reflects the topological features of a particular device as well as the bias conditions. The DF function enters the corresponding rates of the bond depassivation processes via the carrier acceleration integral (AI),

$$I_{SP} = \int_{E_{th,SP}}^{\infty} f(E)g(E)\sigma_{SP}(E)v(E)dE,$$

$$I_{MP} = \int_{E_{th,MP}}^{\infty} f(E)g(E)\sigma_{MP}(E)v(E)dE. \quad (1)$$

The integrand in Eq. (1) is obtained via the multiplication of the carrier flux with energies in the range $[E;E+dE]$ by the probability to launch the reaction by a carrier with such an energy. This flux is just the product of the carrier distribution $f(E)$, density of states $g(E)$, and velocity $v(E)$. Therefore, the SP- and MP-related acceleration integrals have the same functional structure and differ only in their parameters. The carrier energy distribution function $f(E)$ is calculated using the full-band Monte Carlo device simulator. $E_{th,SP}/E_{th,MP}$ are (different) threshold energies of the SP/MP processes and σ_{SP}/σ_{MP} are the Keldysh-like reaction cross sections[8,9]—i.e., of the form $\sigma_{SP}(E)=\sigma_{SP,0}(E-E_{th,SP})^{p_{SP}}$ (the cross section for the MP process has the same structure). In the case of the single-particle bond breakage this means the excitation of the bonding electron to an antibonding state while for the multivibrational mode excitation this reaction is linked to the excitation/decay of the phonon modes.[8,9]

In order to find the interface state generation rate corresponding to the SP process the acceleration integral is multiplied by the attempt rate ν_{SP}, i.e., $\lambda_{SP}=\nu_{SP}I_{SP}$. Assuming the process to follow first-order kinetics, one obtains the following dependence of the SP-related interface state density N_{SP} on time:

$$N_{SP}(t) = n_0[1-\exp(-\lambda_{SP}t)], \quad (2)$$

where n_0 is the concentration of the passivated Si–H bonds which can be broken. The situation with the MP process is more complicated because this process is linked to the excitation of the phonon modes by a cascade of subsequent bombardments of the interface by carriers.[4,5,8,9] Note that the Si–H bond can relax from an excited state to a lower one and a reciprocal process is to be considered as well. Therefore, the bond is treated as a truncated harmonic oscillator (Fig. 1) characterized by a ladder of bonded levels. The last level is designated as N_l. The Si–H bond-breakage process is described by the system gradually climbing the ladder of energetic states, a process which is eventually terminated when the hydrogen atom leaves the last bonded level toward the transport state (Fig. 1). The reaction rate is defined by the height of the barrier E_{emi} which separates the last level N_l and the transport state. Similarly, the passivation process is related to the hydrogen atom jumping into the opposite direction, determined by the barrier height E_{pass}. The corresponding rates (P_{emi}, P_{pass}) are assumed to obey on the Arrhenius law,

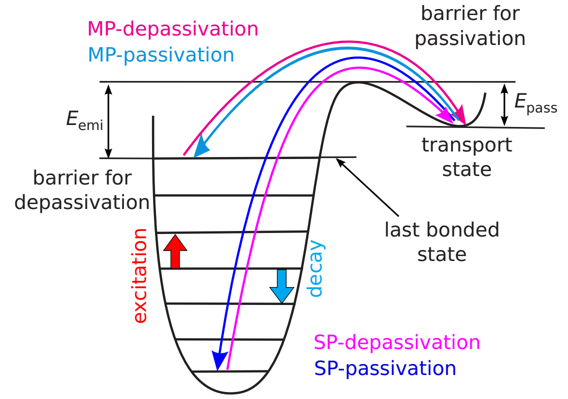

FIG. 1. (Color online) Schematic representation of the SP and MP processes.

$$P_{emi} = \nu_{emi}\exp(-E_{emi}/kT),$$

$$P_{pass} = \nu_{pass}\exp(-E_{pass}/kT), \quad (3)$$

where ν_{emi} and ν_{pass} are attempt frequencies, k is the Boltzmann constant, while T is the lattice temperature.

To obtain an expression for the phonon excitation and decay rates P_u and P_d (Fig. 1), we follow the formalism described in the papers by Hess and co-workers.[8,9] The carrier flux can induce either phonon absorption (i.e., the bond heating) or phonon emission (related to the multivibrational mode decay). Therefore, in these absorption and emission rates, which are just the product of the electron flux, the process capture cross section is divided by the phonon occupation number plus one or by the occupation number, respectively. Since the reaction cross section is energy dependent, the carrier flux differential should be rewritten in a manner indicating that the electron packet contains particles with different energies, i.e., expressed via the acceleration integral. Summarizing all these considerations one obtains the expression for P_u and P_d similarly to Eqs. (10) and (11) as[9]

$$P_u = w_e\exp(-\hbar\omega/kT) + I_{MP},$$

$$P_d = w_e + I_{MP}, \quad (4)$$

with w_e being the phonon frequency and $\hbar\omega$ being the distance between the oscillator levels. The first two terms just describe the population of the oscillator levels in the absence of carrier acceleration while in the presence of the electron flux an additional term I_{MP} enters the expression.

The kinetics of the MP process is determined by a system of rate equations (see, e.g., Ref. 4),

Author complimentary copy. Redistribution subject to AIP license or copyright, see http://jvb.aip.org/jvb/copyright.jsp

TABLE I. Crucial parameters of the stretching and bending vibrational modes of the Si–H bond.

Parameters	Stretching	Bending
E_b (eV)	2.5	1.5
$\hbar\omega$	0.25	0.075
w_e (ps^{-1})	1/295	1/10

$$\frac{dn_0}{dt} = P_d n_1 - P_u n_0, \tag{5}$$

$$\frac{dn_i}{dt} = P_d(n_{i+1} - n_i) - P_u(n_i - n_{i-1}), \tag{6}$$

$$\frac{dn_{N_l}}{dt} = P_u n_{N_l-1} - P_d n_{N_l} - P_{emi} n_{N_l} + \widetilde{P}_{pass} N_{MP}^2. \tag{7}$$

Contrary to Ref. 4, we maintain all four terms in Eq. (7): the first two are related to the oscillator excitation/deexcitation, while the last two control the bond rupture and passivation process. We assume that the MP-related interface state concentration is equal to the density of the mobile hydrogen atoms which are species for the bond passivation reaction. As a result, N_{MP} enters Eq. (7) in the second power. To satisfy the dimensionality we use in Eq. (7) $\widetilde{P}_{pass} = P_{pass}/n_0$.

The model furthermore assumes that a steady state between the individual energy levels is established rather quickly, much quicker than the hydrogen hopping step (depassivation/passivation). As a consequence, these reactions can be considered quasi-independently. Thus, first the last two terms in Eq. (7) are omitted and we consider the oscillator in equilibrium. Consequently, $dn_i/dt = 0$ for each i and recurrently find that $(n_i/n_0) = (P_u/P_d)^i$. For the sake of simplicity we also assume that the oscillator is predominantly in its ground state, i.e., $n_0 = \Sigma_i n_i$. Then we "switch on" hydrogen transitions and obtain the interface state evolution with time,

$$N_{MP} = n_0 \left\{ \frac{\lambda_{emi}}{P_{pass}} \left(\frac{P_u}{P_d} \right)^N [1 - \exp(-\lambda_{emi} t)] \right\}^{1/2}. \tag{8}$$

It is worth emphasizing that in the case of weak stresses and/or short stress time, i.e., when $\lambda_{emi} t \ll 1$, expression (8) transforms to the square root time dependence of N_{MP} as reported in Ref. 4.

The two main Si–H vibrational modes are the stretching and bending modes,[4,23] with their parameters listed in Table I. It has been previously shown[3] that experimental data are better fitted by the bending mode and therefore for our simulations we use the parameters of this mode.

In Ref. 24 we have demonstrated that the SP and MP processes lead to two types of traps which have to be differently distributed over energy in order to match the experimental data. Therefore, we consider these mechanisms independently; i.e., the total interface state density is calculated as a superposition of SP- and MP-related components weighted with corresponding probabilities,

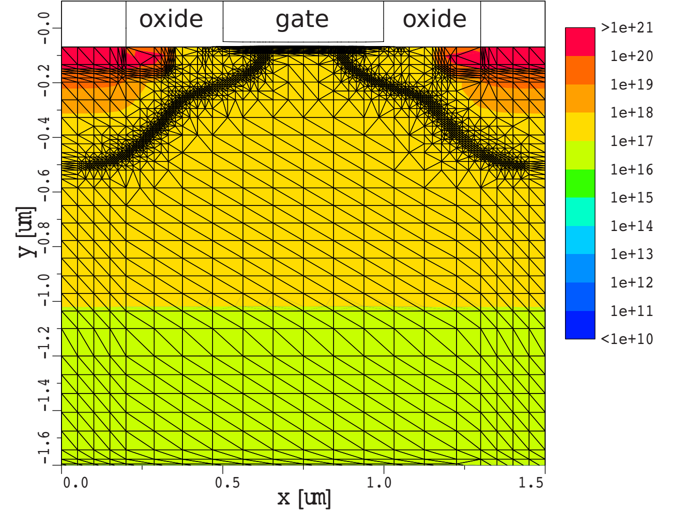

FIG. 2. (Color online) Schematic representation of the n-MOSFET used in this study. The donor concentration is shown by the color map.

$$N_{it} = p_{SP} N_{SP} + p_{MP} N_{MP}. \tag{9}$$

III. EXPERIMENTAL SETUP AND CARGE-PUMPING TECHNIQUE

For the investigation of hot-carrier degradation we use a 5 V n-metal-oxide-semiconductor field-effect transistor (MOSFET) fabricated by a standard 0.35 μm process. The device cross-section/contour plot is schematically depicted in Fig. 2. Since we are dealing with a long-channel device with a length of ~0.5 μm and a relatively high operation voltage of 5 V, one can expect the SP process to dominate the degradation. The devices were stressed at a gate voltage V_{gs} of 2.0 V and source-drain voltage $V_{ds} = 6.75$ V. The ambient temperature was $T = 40$ °C and the stress time $t = 10^5$ s.

To obtain the experimental interface state profile, the constant base-level charge-pumping technique has been employed.[25–30] In our work we use a standard experimental scheme where the gate of the transistor is connected to a pulse generator and a small constant reverse bias is applied to the source and drain. The measured current is the substrate current (I_{cp}). We use with $V_{gl} = -5$ V and increase V_{gh} from −4 to 4 V in 0.004 V increments, where V_{gl} and V_{gh} are the base and the high levels of the gate pulse, respectively (see inset of Fig. 3). Such a small voltage step is required in order to obtain sufficient spatial resolution. For the extraction of the N_{it} profile from the CP current we employ the approach suggested in Refs. 26, 29, and 31. The interface trap concentration can be written as[26]

$$N_{it}(x) = \frac{1}{qfW} \frac{dI_{cp,d}(V_{gh})}{dV_{gh}} \frac{dV_{th}(x)}{dx}. \tag{10}$$

Here, the reasonable assumption[27,31] that the source and drain are symmetric for the fresh device and the damage is

Author complimentary copy. Redistribution subject to AIP license or copyright, see http://jvb.aip.org/jvb/copyright.jsp

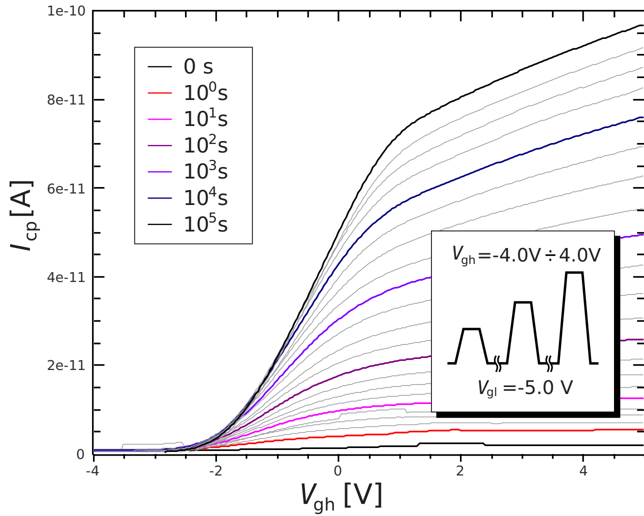

FIG. 3. (Color online) Time evolution of the measured I_{cp}-V_{gh} relationship during hot-carrier stress using the constant base-level charge-pumping technique. The inset shows a schematic gate pulse train.

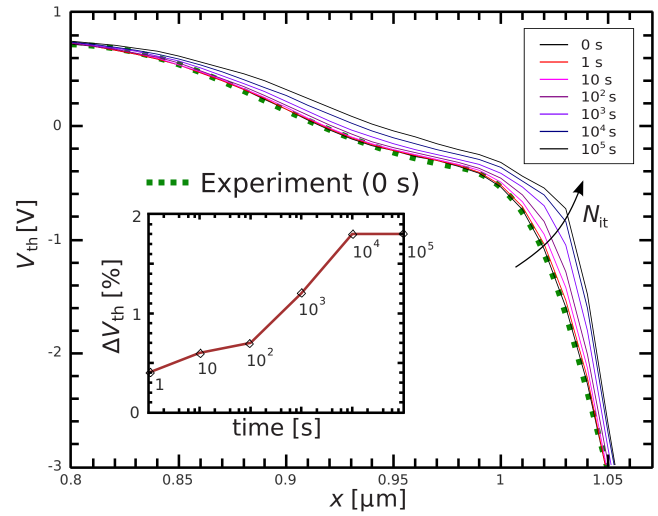

FIG. 4. (Color online) Local threshold voltage $V_{th}(x)$ along the channel before and after the stress. For the fresh device, simulation results are in good agreement with experiment (green dotted line). The shift of the threshold voltage ΔV_{th} measured by the maximum transconductance method is shown in the inset.

induced only near the drain side is employed. Thus, it is possible to separate the part of I_{cp} corresponding to the increase of the N_{it} concentration from the total one,

$$I_{cp,d}(V_{gh}) = I_{cp}(V_{gh}) - \frac{I_{cp,0}(V_{gh})}{2}, \tag{11}$$

where $I_{cp,0}$ is the CP current of the unstressed device. The dependence of the threshold voltage on the coordinate along the interface x is determined by the doping concentration, the oxide thickness, and the amount of charges in the oxide. For the fresh device $V_{th}(x)$ can be calculated with our device simulator MINIMOS-NT using a widely adopted routine.[26,31–34] Namely, the local threshold voltage of a point at the interface is defined as the gate voltage required to accumulate the electron concentration n_e,[32]

$$n_e = \frac{1}{v_{th}\sigma_e\tau_e}, \tag{12}$$

where v_{th} is thermal carrier velocity ($=1\times10^7$ cm/s), τ_e is time constant for electron trapping ($=1/2f$), and σ_e is capture cross section for electrons[35] ($=3.9\times10^{-16}$ cm^2).

For a gate pulse with a frequency of $f=25$ kHz, we have $n_e=1.3\times10^{13}$ cm^{-3}. The soundness of the obtained result has been checked by the method proposed in Refs. 27 and 34. According to this approach it is possible to extract the dependence of the local threshold voltage on the interface coordinate directly from the charge-pumping current $I_{cp,0}(V_{gh})$ for the undamaged device,[27]

$$V_{th}(x) = V_{gh}, \quad x(V_{gh}) = x_{Lc} + \left[1 - \frac{I_{cp,0}(V_{gh})}{I_{cp,0,max}}\right](x_{Ld} - x_{Lc}). \tag{13}$$

Here, the center point of the channel x_{Lc} depends on the gate mask length and x_{Ld} is the channel end point on the drain side that can be detected with the CP method.[27,34] A comparison between the experimental and the simulated threshold voltage profiles $V_{th}(x)$ is shown in Fig. 4.

The threshold voltage $V_{th}(x)$ remains unchanged during HC stress only if the influence of the interplay between oxide and interface charges is small enough.[26,31,34] Otherwise, necessary corrections of $V_{th}(x)$ after each stress time step have to be performed, which is rather complicated for MOSFETs with a nonuniform channel doping profile.[26–30,34] In Refs. 28–30 and 33 the impact of the bulk oxide trap Q_{ot} and interface trap density N_{it} on the CP current has been analyzed. A change in $Q_{ot}(x)$ without changing $N_{it}(x)$ results only in a local shift of I_{cp} along the V_{gh} axis. On the other hand, an increase of $N_{it}(x)$ without changing $Q_{ot}(x)$ will only cause a local increase of dI_{cp}/dV_{gh}. Thus, based on the shape evolution of the I_{cp} and dI_{cp}/dV_{gh} curves for different HC stress times we believe that no significant amount of oxide charges was generated under these stress conditions. This fact was confirmed by measurements of the threshold voltage shift ΔV_{th} by the maximum transconductance method (see inset of Fig. 4). The increase of ΔV_{th} demonstrates the dominance of N_{it} generation. Thus, it is possible to use a simplified method for N_{it} extraction and consider only the effect of N_{it} on the calculated V_{th} (shown in Fig. 4),

$$V_{th}(x) = V_{th,0}(x) + \frac{q\Delta N_{it}(x)}{2C_{ox}}, \tag{14}$$

where C_{ox} is the oxide capacitance per unit

IV. RESULTS AND DISCUSSION

We calibrated the model in order to represent the N_{it} profile extracted from CP data (Fig. 5). For the SP and MP components we have chosen different parameters controlling the corresponding carrier acceleration integrals, which eventually lead to substantially different dependences of the ac-

Author complimentary copy. Redistribution subject to AIP license or copyright, see http://jvb.aip.org/jvb/copyright.jsp

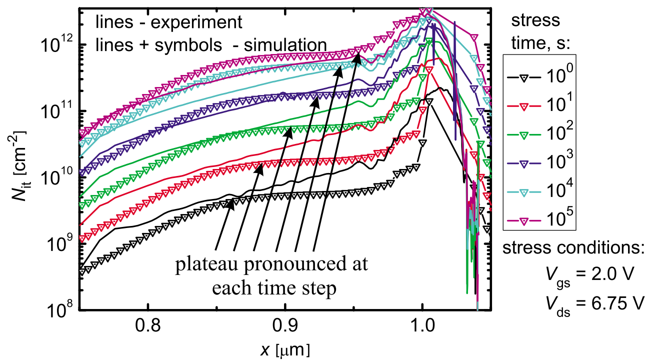

FIG. 5. (Color online) Interface state density vs coordinate x for several stress times: experiment vs theory.

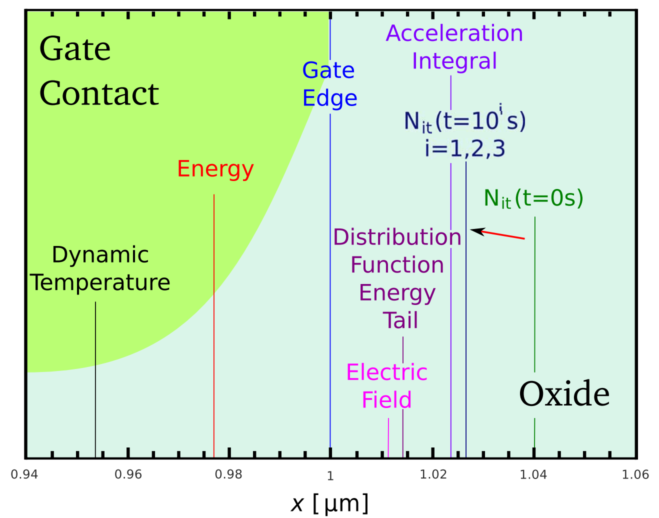

FIG. 6. (Color online) Position of the different physical quantity maxima and interface state profile peak.

celeration integrals on the lateral coordinate. Usually it is accepted that the severest spot of hot-carrier degradation is localized in the position where the electric field (or the driving force) peaks. This is because close to this area carriers gain their maximal energy and the Si–H bond dissociation process is most intensive. However, the maxima of such physical quantities as the electric field, electron energy, or carrier temperature are, in fact, never at the same position. Moreover, since both SP and MP processes are controlled by the acceleration integrals, probably just the maxima of these integrals correspond to the N_{it} peak. The acceleration integral maximum is defined by the shape of the distribution function or—more precisely—by the depth of the high-energy tails. Therefore, the device area where most extended tails of the DF are observed is situated close to the position of the highest degradation dose. Finally, as we showed previously,[20] the spatial position of the most severe spot determined according to different criteria is shifted, respectively, to each other. To conclude, it is very important to compare the coordinates of the most intensive trap creation determined according to different criteria and the maxima of N_{it} (as well as N_{it} peak for the undamaged device). This information is provided by Fig. 6. The unstressed device is characterized by the preexisting interface state density and the initial N_{it} has a peak at a certain position depending on the fabrication process. This results in a shift of the interface state density profile maximum during the first few seconds of the degradation (Fig. 6). After 10 s of hot-carrier stress the peak of the experimental N_{it} profile practically coincides with the peak of I_{SP} (peak of the theoretical N_{it}). Such a system behavior depicted in Fig. 6 makes it possible to conclude that the description of the hot-carrier degradation is impossible just in the framework of such quantities as electric field, dynamic temperature, carrier energy, etc. Figure 6 shows that the peak positions are distributed in space and the extension of these distribution is about 100 nm which is already rather large (especially compared to the distance between the N_{it} and AI maxima). Moreover, these results once again confirm that the maximum of the interface state profile should be described in terms of the AI rather than by the position of the deepest high-energy tail of the distribution function.[16,17] Both SP and MP mechanisms of Si–H bond breakage are described by the carrier AI controlled by the DF. The structure of the integrand contains a superposition of rapidly decaying high-energy tails of the distribution function and a rapidly increasing combination of capture cross section, carrier velocity, and density of states. Therefore, the maximum of this integral shifted the position where the DF demonstrates deepest high-energy tails, which corresponds to the findings in Ref. 20.

After 10^3 s we observe a weak second shift ($\sim$17 nm) of the N_{it} peak toward the drain contact side. This may be attributed to the distortion of the DF due to the interface state creation (which is not considered during the simulations) or to the influence of Q_{ot} buildup. Figure 7 demonstrates a strong localization of the degradation portion associated with the single-particle process. Corresponding to the SP mechanism, the AI abruptly changes practically from 0 to a significant value resulting in N_{SP} buildup [compare with Fig. 8(a)]. In contrast, the MP-related acceleration integral changes not so drastically with the coordinate. Three pronounced humps in the profile mimic the energy tails of the DF. The first (centered at $x \approx 0.25$ μm) and the third (positioned at ≈ 1.25 μm) humps are associated with the p-n junctions of

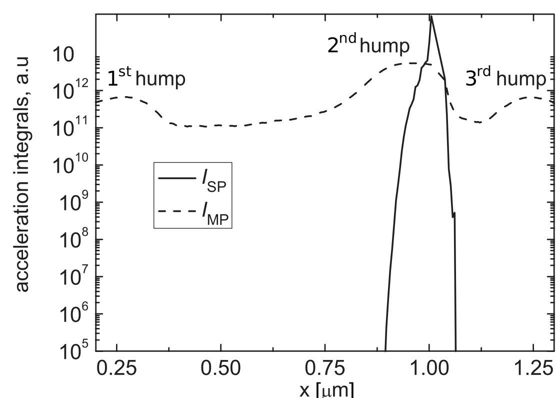

FIG. 7. Dependence of the acceleration integral for the SP (solid line) and MP (dashed line) processes. Integrals are given in arbitrary units.

Author complimentary copy. Redistribution subject to AIP license or copyright, see http://jvb.aip.org/jvb/copyright.jsp

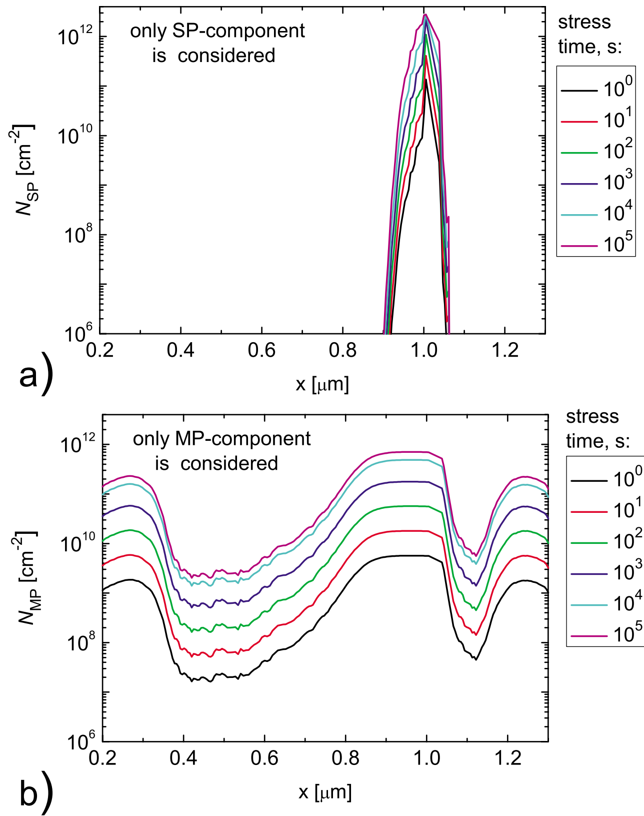

FIG. 8. (Color online) SP- and MP-related components of the total interface state density plotted vs the lateral coordinate.

the source/channel and channel/drain sections of the MOSFET, while the second one is observed near the drain end of the gate, i.e., just near the areas where the DF has its deepest high-energy tails. This tendency is reflected on the SP- and MP-induced interface state profiles plotted in Figs. 8(a) and 8(b), respectively.

Note that the AI for the MP process controls the interface state density via the prefactor (P_u/P_d) in expression (8) and thus its variation is not as large as in the case of the SP component. Figure 8(b) shows that N_{MP} represents the behavior of the corresponding AI. This means that electrons in the channel cannot reach high energies in this range and are cold from the perspective of the SP process but still have sufficient energy in order to contribute to the MP mechanism. To conclude, the MP component is present along the whole distance, in contrast to the SP component which contributes only in a rather narrow region. It should be noticed that just N_{MP} is responsible for the flat plateau situated left to the maximum of the total concentration N_{it} (this plateau is schematically shown in Fig. 5).

It is worth commenting on the choice of parameters entering the acceleration integral. For the SP process we employed parameters similar to those reported in previous papers (e.g., Refs. 4, 5, 8, and 9): the threshold energy for the bond-breakage process is set equal to $E_{th,SP}=1.5$ eV and the exponent in the Keldysh-like reaction cross section $p_{it,SP}=11$. The parameters characterizing the energetics of the truncated harmonic oscillator were similar to those listed in Table I. However, we fitted experimental data with our simulations taking $p_{it,MP}\sim 0.1$, i.e., assuming the process to be practically energy independent. Actually, $p_{it,SP}$ and $p_{it,MP}$ describe different physical processes, i.e., the excitation of the bonding electron to the antibonding state in the former case and electron-phonon interaction in the latter one. Generally speaking, these processes are described by different values of reaction cross sections. The value of $E_{th,MP}$ equal to 1.5 eV used in the model should be also checked because it is also inherited from the SP process. Although the pair of parameters $p_{it,MP}\sim 0.1$, $E_{th,MP}=1.5$ eV satisfactorily describe the matter, this issue has to be clarified. A weak energy dependence of the cross section for the MP process may also be related to the parameter dispersion when the large standard deviation dictates that a smaller value of the parameter makes the main contribution. Note also that for both processes the dispersion of the parameters—first of all the threshold energy and the cross section (e.g., Refs. 17 and 36)—also impacts the energetics and the effective value of a parameter may be substantially different with respect to the mean one.

Due to the stochastic nature of the Monte Carlo method, calculation of the distribution function with a good spatial resolution and accurate high-energy tails is a time-consuming challenge. Additionally, a refinement may be achieved in the extraction technique of the N_{it} profile from CP data. In Eq. (13) we consider C_{ox} to be constant, which could work only as a first-order approach. The presence of oxide and/or interface charges transforms C_{ox} into a function of the interface coordinate. Moreover, Eq. (11) implies that the buildup of the interface traps takes place only near the drain region of the transistor. Such an idealistic assumption is applicable only for a narrow set of the stress voltages. Otherwise, a more complicated experimental scheme with separated source and drain parts of the CP current should be employed (e.g., see Ref. 37).

Already at the present stage we emphasize the necessity of a self-consistent procedure for the extraction of the N_{it} profile from CP measurements. After each time step of the HC stress the influence of N_{it} and Q_{ot} on the threshold and/or flat band voltages should be taken into account. Otherwise, a discrepancy between the extracted and the experimental values of N_{it} could amount up to one order of magnitude.

V. CONCLUSION

A comprehensive physics-based model for hot-carrier degradation has to consider three different aspects: the carrier transport, the microscopic description of the defect buildup, and the impact of the generated defects on the device performance. While exchanging the information between these blocks one should perform a thorough check at each stage. We have carried out a direct analysis of the interface state density profile assessed within our model and that extracted from charge-pumping measurements. To model the interface state density profile we rely on a thorough evaluation of the carrier energy distribution function by means of a full-band Monte Carlo device simulator. We have

Author complimentary copy. Redistribution subject to AIP license or copyright, see http://jvb.aip.org/jvb/copyright.jsp

considered the interplay between hot and colder carriers or—in other words—the interplay between the single- and multiple-carrier components of the Si–H bond breakage. The importance of the MP component even in the case of long-channel devices and relatively high stress voltages was demonstrated.

The carrier acceleration integrals for the SP and MP processes are characterized by rather different profiles. In particular, the SP component is strongly localized near the drain end of the gate electrode, while the MP component is more or less homogeneously distributed. The latter means that under high stress conditions the MP mechanism that is still triggered is linked with the low-energy part of the distribution function.

Note that for the calculation of the SP-related acceleration integral we used just the same parameter set as was used in the papers by Bravaix and co-workers,[4,5] while for the MP component in the Keldysh-like reaction cross section the exponent of 0.1 (i.e., process is only slightly sensitive to the carrier energy variations) has been used. Such a small value of $p_{\mathrm{it,MP}}$ may be attributed to the dispersion of the parameters of the Si–H bond energetics repeatedly reported in the literature.[17,36]

[1] A. Acovic, G. La Rosa, and Y. C. Sun, Microelectron. Reliab. **36**, 845 (1996).
[2] L. Hong, Ph.D. thesis, National University of Singapore, 2005.
[3] M. P. Pagey, MS thesis, Vanderbilt University, 2002.
[4] A. Bravaix, C. Guerin, V. Huard, D. Roy, J. M. Roux, and E. Vincent, Proceedings of the IRPS, 2009 (unpublished), pp. 531–546.
[5] C. Guerin, V. Huard, and A. Bravaix, J. Appl. Phys. **105**, 114513 (2009).
[6] H. Kufluoglu and M. A. Alam, J. Comput. Electron. **3**, 165 (2005).
[7] H. Kulfuoglu, Ph.D. thesis, Purdue University, 2007.
[8] K. Hess, L. F. Register, B. Tuttle, J. Lyding, and I. C. Kizilyalli, Physica E (Amsterdam) **3**, 1 (1998).
[9] W. McMahon, K. Matsuda, J. Lee, K. Hess, and J. Lyding, Technical Proceedings of the 2002 International Conference on Modeling and Simulation of Microsystems (2002), p. 576.
[10] K. O. Jeppson and C. M. Svensson, J. Appl. Phys. **48**, 2004 (1977).
[11] M. A. Alam and S. Mahapatra, Microelectron. Reliab. **45**, 71 (2005).
[12] T. Grasser, W. Gos, and B. Kaczer, IEEE Trans. Device Mater. Reliab. **8**, 79 (2008).
[13] T. Grasser, W. Gös, and B. Kaczer, ECS Trans. **19**(2), 265 (2009).
[14] T. Grasser *et al.*, Proceedings of the IEDM, 2010 (unpublished).
[15] K. Hess, I. C. Kizilyalli, and J. W. Lyding, IEEE Trans. Electron Devices **45**, 406 (1998).
[16] W. McMahon, A. Haggaag, and K. Hess, IEEE Trans. Nanotechnol. **2**, 33 (2003).
[17] A. Haggag, W. McMahon, K. Hess, K. Cheng, J. Lee, and J. Lyding, Proceedings of the IRPS, 2001 (unpublished), pp. 271–279.
[18] O. Penzin, A. Haggag, W. McMahon, E. Lyumkis, and K. Hess, IEEE Trans. Electron Devices **50**, 1445 (2003).
[19] S. E. Tyaginov *et al.*, Proceedings of the IPFA, 2010 (unpublished).
[20] I. A. Starkov *et al.*, Proceedings of the IPFA, 2010 (unpublished).
[21] C. Jungemann and B. Meinerzhagen, *Hierarchical Device Simulation* (Springer Verlag, New York, 2003).
[22] MINIMOS-NT device and circuit simulator, Institute for Microelectronic, TU Wien.
[23] R. Biswas, Y.-P. Li, and B. C. Pan, Appl. Phys. Lett. **72**, 3500 (1998).
[24] S. E. Tyaginov *et al.*, Microelectron. Reliab. **50**, 1267 (2010).
[25] A. B. M. Elliot, Solid-State Electron. **19**, 241 (1976).
[26] S. S. Chung and J.-J. Yang, IEEE Trans. Electron Devices **46**, 1371 (1999).
[27] R. G.-H. Lee, J.-S. Su, and S. S. Chung, IEEE Trans. Electron Devices **43**, 81 (1996).
[28] H.-H. Li, Y.-L. Chu, and C.-Y. Wu, IEEE Trans. Electron Devices **44**, 782 (1997).
[29] C. Chen and T. P. Ma, IEEE Trans. Electron Devices **45**, 512 (1998).
[30] Y.-L. Chu, D.-W. Lin, and Ch.-Y. Wu, IEEE Trans. Electron Devices **47**, 348 (2000).
[31] S. Okhonin, T. Hessler, and M. Dutoit, IEEE Trans. Electron Devices **43**, 605 (1996).
[32] P. Heremans, J. Witters, G. Groeseneken, and H. E. Maes, IEEE Trans. Electron Devices **36**, 1318 (1989).
[33] P. Moens, F. Bauwens, M. Nelson, and M. Tack, Proceedings of the IRPS, 2005 (unpublished), pp. 555–559.
[34] M. Tsuchiaki, H. Hara, T. Morimoto, and H. Iwai, IEEE Trans. Electron Devices **40**, 1768 (1993).
[35] D. Bauza, J. Appl. Phys. **94**, 3239 (2003).
[36] K. Hess, A. Haggag, W. McMahon, K. Cheng, J. Lee, and J. Lyding, IEEE Circuits Devices Mag. **17**, 33 (2001).
[37] W. K. Chim, S. E. Leang, and D. S. H. Chan, J. Appl. Phys. **81**, 1992 (1997).

Author complimentary copy. Redistribution subject to AIP license or copyright, see http://jvb.aip.org/jvb/copyright.jsp